Geoderma 343 (2019) 269–279

Contents lists available at ScienceDirect

Geoderma

journal homepage: www.elsevier.com/locate/geoderma

Is it possible to map subsurface soil attributes by satellite spectral transfer models?

Wanderson de S. Mendes[a], Luiz G. Medeiros Neto[a], José A.M. Demattê[a,*], Bruna C. Gallo[b], Rodnei Rizzo[c], José L. Safanelli[a], Caio T. Fongaro[a]

[a] Department of Soil Science, College of Agriculture Luiz de Queiroz, University of São Paulo, Piracicaba, São Paulo State, Brazil
[b] Bioenergy Program, University of Campinas, Campinas, São Paulo State, Brazil
[c] Center of Nuclear Energy in Agriculture, University of São Paulo, Piracicaba, São Paulo State, Brazil

ARTICLE INFO

Handling Editor: Alex McBratney

Keywords:
Geographically weighted regression
Multitemporal bare soil image
Proximal sensing
Soil prediction
Subsurface soil mapping

ABSTRACT

It is impossible to make pedological maps without understanding subsurface attributes. Several strategies can be used for soil mapping, from a tacit knowledge to mathematical modeling. However, there are still gaps in knowledge regarding how to optimize subsurface mapping. This work aimed to quantify subsurface soil attributes using satellite spectral reflectance and geographically weighted regression (GWR) techniques. The study was carried out in São Paulo, Brazil, in an area spanning 47,882 ha. Multitemporal satellite images (Landsat-5) were initially processed in order to retrieve spectral reflectance from the bare soil surface. Based on a toposequence method, 328 points were then distributed across the area (at depths between 0 and 20 cm and 80 and 100 cm) and analyzed for their soil chemical and physical attributes (including the reflectance spectra (400 to 2500 nm)) in the laboratory. We achieved 67.72% of bare soil for the whole study area, with the remaining 32.28% of the unmapped surface being filled by kriging interpolation. All 328 samples were modeled using surface (Landsat-5 TM spectral reflectance) and subsurface (acquired in the laboratory) data, reaching up to 0.72 R^2_{adj}. The correlation between the spectra of both depths was significant and the soil attributes prediction reached an R^2_{adj} of validation above 0.6 for clay, hue, value, and chroma at 0–20 and 80–100 cm depths. The satellite soil surface reflectance allowed the estimation of soil subsurface attributes. These results demonstrate that diagnostic soil attributes can be quantified based on spectral pedotransfer (SPEDO) functions to assist digital soil mapping and soil monitoring. Despite our efforts to determine soil subsurface properties using digital soil mapping approach, this task still need considerable refinement. Thus, research must continue to aggregate outcomes from other techniques.

1. Introduction

Classical soil mapping fundamentally depends on the surveyor's knowledge of the relationships between soil-forming factors (Jenny, 1941), and is based on standard sampling densities to boost its efficiency. The surveyor's criteria are not precise due to the absence of a clear modeling method (Miller and Schaetzl, 2016). An initial solution to this arose when McBratney et al. (2003) introduced the concept of Digital Soil Mapping (DSM) to integrate advanced mathematical techniques with classical soil survey methods. However, an important component of all soil classification systems is the diagnostic horizons (Bockheim et al., 2014; IUSS Working Group WRB, 2015; Soil Survey Staff, 2014), and it is impossible to make a pedological map without understanding the subsurface attributes (diagnostic horizons). Soil property data from the subsurface is directly related to diagnostic horizons, which drives many soil classification systems (IUSS Working Group WRB, 2015; Soil Survey Staff, 2014).

Abbreviations: SPEDO, spectral pedotransfer functions; GWR, geographically weighted regression; MLR, multiple linear regression; GEOS3, geospatial soil sensing system; SYSI, synthetic soil image; TM, thematic mapper sensor of Landsat 5; KGSYSI, a bare soil image generated by kriging the SYSI values; KGOSYSI, a bare soil image combining the original SYSI and kriging estimates for the non-filled gaps; R, Munsell's red color; YR, Munsell's red-yellow color; Y, Munsell's yellow color; OM, organic matter; CEC, cation exchange capacity; CA, clay activity; Ta, high activity clays; Tb, low activity clays; V%, base saturation; BS, sum of bases; m%, aluminum saturation; Vis, visible region of the electromagnetic spectrum; NIR, near infrared region of the electromagnetic spectrum; SWIR, shortwave infrared of the electromagnetic spectrum; BSSIKG, estimated subsurface spectral reflectance from KGSISY; BSSIKGO, estimated subsurface spectral reflectance from KGOSYSI; RMSE, root mean square error; R^2, coefficient of determination; RPIQ, ratio of performance to interquartile range; RPD, ratio of performance to deviation; RGB, red, green and blue channels for image composites

* Corresponding author.
E-mail address: jamdemat@usp.br (J.A.M. Demattê).

https://doi.org/10.1016/j.geoderma.2019.01.025
Received 7 December 2017; Received in revised form 24 September 2018; Accepted 8 January 2019
Available online 27 February 2019
0016-7061/

Pedological surveys at a large scale are essential, but high costs and lack of manpower are serious constraints. DSM can be used to mitigate the problems, as indicated by McBratney et al. (2003). DSM utilizes field, laboratory, and soil information and interprets relationships by using quantitative methods to predict patterns at various temporal and spatial scales (Grunwald, 2010). These methods estimate characteristics at unknown locations using known patterns, correlated with satellite spectra and/or relief data, using multivariate techniques. Therefore, soil attributes can be estimated from satellite images and/or relief data (Franceschini et al., 2015; Gerighausen et al., 2012; Moore et al., 1993; Mulder et al., 2011; Odeh et al., 2006).

The spectral library is another important tool and is defined as a dataset of soil samples with their respective laboratory and spectral analyses attributes (Viscarra Rossel et al., 2016a, 2016b). For a soil sample, the spectrum obtained can provide many properties using empirical modeling. This methodology has been successfully used by several researchers (Khayamim et al., 2015; Viscarra Rossel et al., 2010a, 2010b). Additionally, soil mapping requires many samples to be taken in order to estimate their attributes and these will be distributed across the landscape, to allow estimation of the spatial variability of the soil properties.

Understanding the role of spatial variations in surface and subsurface soil is essential for decision-making in the fields of sustainable agriculture and environmental monitoring. Agbu et al. (1990) demonstrated the correlation between surface and subsurface soil properties by showing spectral associations between underlying layers and the pedogenetic influence of subsurface properties. Galvão et al. (1997) investigated the interaction between the subsurface and surface properties of tropical soils from Brazil using spectroscopy. The authors analyzed the color variations and spectral reflectance, in addition to their association with the physicochemical soil constituents.

Some aspects of this approach still need to be explored. Demattê et al. (2009) observed that surface patterns obtained by satellite could discriminate many soil classes. In most cases, only surface attributes have been predicted in studies using satellite images (Demattê et al., 2016; Diek et al., 2017; Shabou et al., 2015) and/or relief (Vasques et al., 2016; Wilford et al., 2016). Subsurface soil information can provide data on things such as organic matter content, cation exchange capacity, soil depth, soil drainage etc., which are imperative for root development and other soil functions. A recent study by Ordóñez et al. (2018) exemplified the importance of understanding subsurface soil attributes for crop development and maximum yield. The authors found that the maximum depth for root development of maize and soybean ranges from 89 to 157 cm.

Since only 5% of Brazil has been mapped at the 1:100,000 scale (Polidoro et al., 2016), it is impossible to perform detailed soil mapping using only traditional field-based and manpower-heavy methods. It is imperative that we shed light on the ways to rapidly estimate subsurface soil attributes. Thus, our main objective was to quantify subsurface soil attributes using soil surface spectral pedotransfer functions, calibrated by satellite information. The hypothesis of the present work is that there is a relationship between surface and subsurface soil properties, as observed by field experience. Even though the surface information is typically associated with the top 3 cm soil layer, subsurface soil spectra can be linked to the surface spectra using a “spectral pedotransfer function” (SPEDO). The concept illustrated here is an extension of traditional pedotransfer functions using spectral information. This approach has the potential to obtain subsurface information for digital soil mapping.

2. Material and methods

2.1. Study site, sampling points, and laboratory spectra

The study site is in a region of the municipality of Rio das Pedras, São Paulo State, Brazil, and covers an area of 47,882 ha. The altitude ranges from 500 to 700 m asl (Fig. 1). The geology of the region is complex (Piracicaba SF 23 - M 300 map, published at a scale 1:100,000 (Mezzalira, 1966)).

The following strata can be observed:

Ct - Carboniferous, Tubarão Group (composed of sandstones, siltstones, varvites, tillites and conglomerates);
Jbp - Jurassic, Botucatu and Pirambóia Formations (comprised of sandstone, siltstones and shales);
Ksg - Cretaceous, Serra Geral Formation (consisting of basalt, sandstone, inter-trap and diabasium); Pc - Permian, Corumbataí Formation (consisting of siltstones, shales, limestone and flint); and.
Pi - Permian, Irati Formation (consisting of shales, pyrobetuminosite, dolomite and siltite (see Fig. 1).

At this site, 328 points were allocated based on the toposequence method and soil samples were collected at depths of 0–20 cm and 80–100 cm. The samples were analyzed by conventional methods for chemical and granulometric estimates (Donagemma et al., 2011). In addition, reflectance spectra were acquired using the Fieldspec Pro (Analytical Spectral Devices, Boulder, Colorado, USA) in the laboratory, according to the methodology described by Terra et al. (2015). In this case, reflectance data were obtained with a spectral resolution of 1 nm, from 350 to 1100 nm, and 2 nm, from 1100 to 2500 nm. Samples were placed on petri dishes and the sensor was positioned vertically, 8 cm from the platform. The sensor detected the energy reflected from two 50-W halogen lamps, positioned 35 cm from the platform with a zenith angle of 30°. The reflectance of a white Spectralon reference plate was measured at the beginning of each set of measurements.

2.2. Bare soil image

A spectral reflectance composite of bare soil retrieved from the multitemporal Landsat-5 TM (Thematic Mapper) archive was used; this was produced by the GEOS3 (Geospatial Soil Sensing System) described in Demattê et al. (2018). Images from 1984 to 2011 and between July and September were processed to produce a bare soil composite, allowing a representation of 67.72% of the bare soil surface of the area. The acquisition dates of the images mentioned above were chosen because they relate to the dry season in the region, which minimized the influence of moisture on the soil surface. The period is also associated with reduced cloud coverage and a higher incidence of bare soil areas.

A brief description of the GEOS3 method is as follows (Fig. 2): (1) creation of a database of atmospherically corrected, surface reflectance images; (2) generation of spectral indices; (3) definition of spectral indices thresholds to separate bare soil from other land cover patterns; (4) extraction of bare soil areas from the database and calculation of an average soil composite. Afterwards, a single multispectral image was obtained and designated as the Synthetic Soil Image (SYSI).

The SYSI still presented large gaps in places where no bare soil was found in the multitemporal archive. Thus, to fill these gaps, we extracted spectral values of SYSI using a 200 × 200 m grid and then interpolated the multispectral reflectance by the geostatistical kriging method (Fig. 2). The grid spacing (200 × 200 m) was used because of the computer processing limitations associated with the size of the area. The Landsat surface reflectance has a known 30 × 30 m pixel resolution, but the size of the mapped area limited the grid spacing to the same resolution as the Landsat images. The kriging estimate was denominated as Kriging from SYSI (KGSYSI). A combined SYSI was produced by combining the original SYSI with the kriging estimates, preserving the original values in 67% of the mapped area and assigning interpolated estimates for the gaps. This aggregated composite was denominated as SYSI overlapped with KGSYSI (KGOSYSI) (Fig. 2).

2.3. Soil attributes

We chose the following soil attributes that are important when classifying soils:

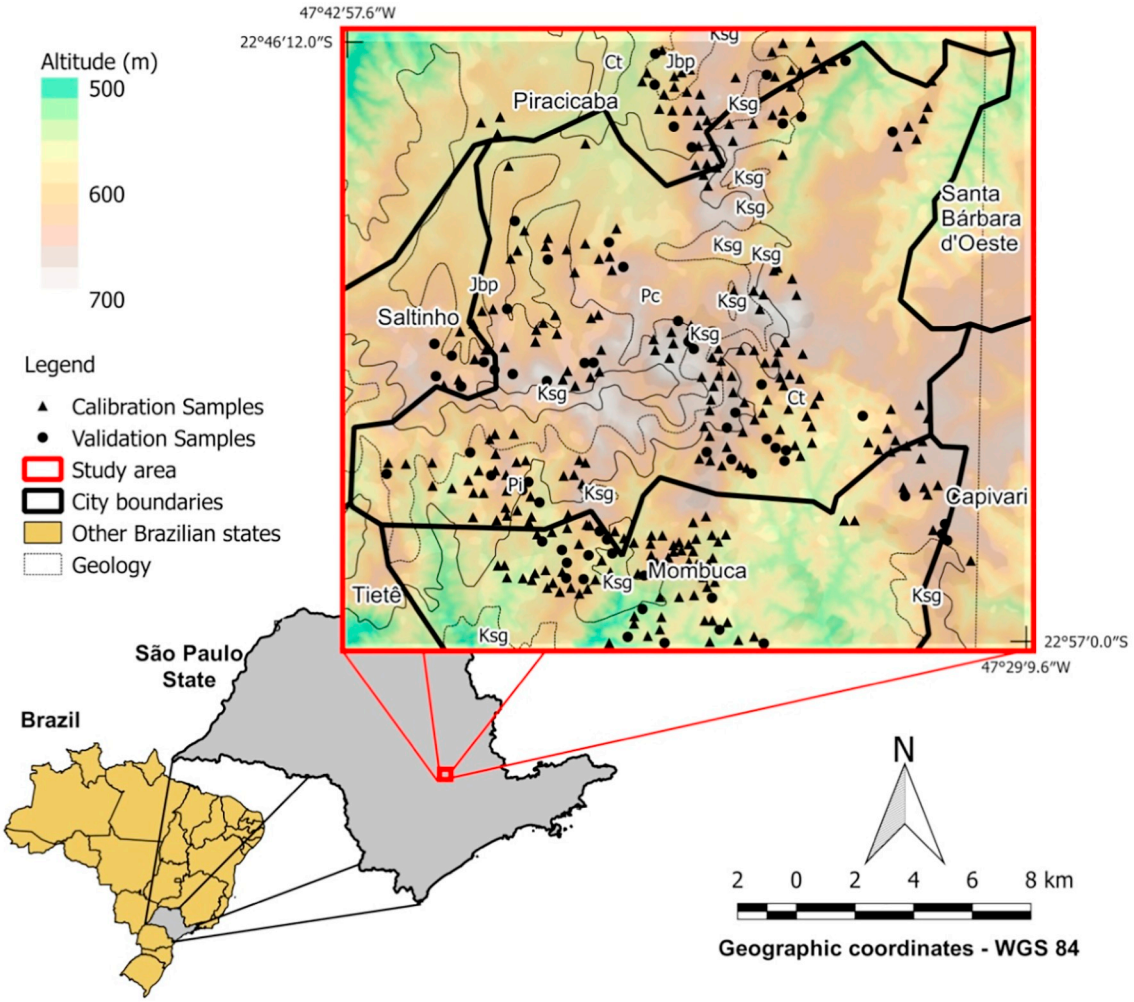

Fig. 1. Location of the study area, distribution of sampling points, and geology of the region combined with a digital elevation model from the Shuttle Radar Topographic Mission 30 m. Ct - Carboniferous, Tubarão Group; Jbp - Jurassic, Botucatu Formation and Pirambóia Formation; Ksg - Cretaceous, Serra Geral Formation; Pc - Permian, Corumbataí Formation, and Pi - Permian, Irati Formation (Mezzalira, 1966).

i. Munsell soil color: represented by the attribute's hue, value, and chroma, between 80 and 100 cm depth (near the diagnostic horizon). This can be related to soil classes such as Ferralsols, Nitosols, and Lixisols (IUSS Working Group WRB, 2015). The hue attribute was transformed into a numerical value, where $R = 0$, YR = 10, and Y = 20.

ii. Clay content for soil texture gradient: defined by the ratio between clay content in the subsurface (80–100 cm) and surface (0–20 cm) layers (dos Santos et al., 2013). This attribute is a key to determining the type of B horizon present. Additionally, the soil texture gradient was calculated from different surface clay classes according to dos Santos et al. (2013).

iii. Organic matter (OM): the surface organic matter is important when classifying Organosols (Histosols) (OM ≥ 13%) and other soils with a chernozemic A horizon (Organic carbon > 6 g kg^{-1} and V % > 65) (dos Santos et al., 2013).

iv. Cation exchange capacity (CEC): this attribute is important when determining high (Ta) and low (Tb) clay activity (CA). Clay activity is calculated by

$$CA = (1000CEC)/clay$$

where *CEC* is given in cmolc kg^{-1} and the *clay* content is given in g kg^{-1}. CEC is classified as Ta if the value is greater than or equal to 27 cmolc kg^{-1} (dos Santos et al., 2013).

v. Base saturation (V%): this is used to determine areas with a eutrophic (V% ≥ 50) or dystrophic (V% < 50) character. It is essential to identifying the chernozemic A horizon (V% > 65, Organic Carbon > 6 g kg^{-1}) and high, relative aluminum content (Al ≥ 4 cmolc kg^{-1}, CA ≥ 20 cmolc kg^{-1}, m% ≥ 50 or V% < 50) and is calculated by

$$V\% = 100BS/CEC$$

where the sum of bases (*BS*) and *CEC* are given in cmolc kg^{-1} (dos Santos et al., 2013).

vi. Aluminum saturation (m%): this is a key to determining areas with high relative aluminum contents (Al ≥ 4 cmolc kg^{-1}, CA ≥ 20 cmolc kg^{-1}, and m% ≥ 50 or V% < 50) and classifying Nitosols (dos Santos et al., 2013). The calculation of *m*% is given by

$$m\% = 100Al/BS + Al$$

where *BS* and *Al* are in cmolc kg^{-1} (dos Santos et al., 2013).

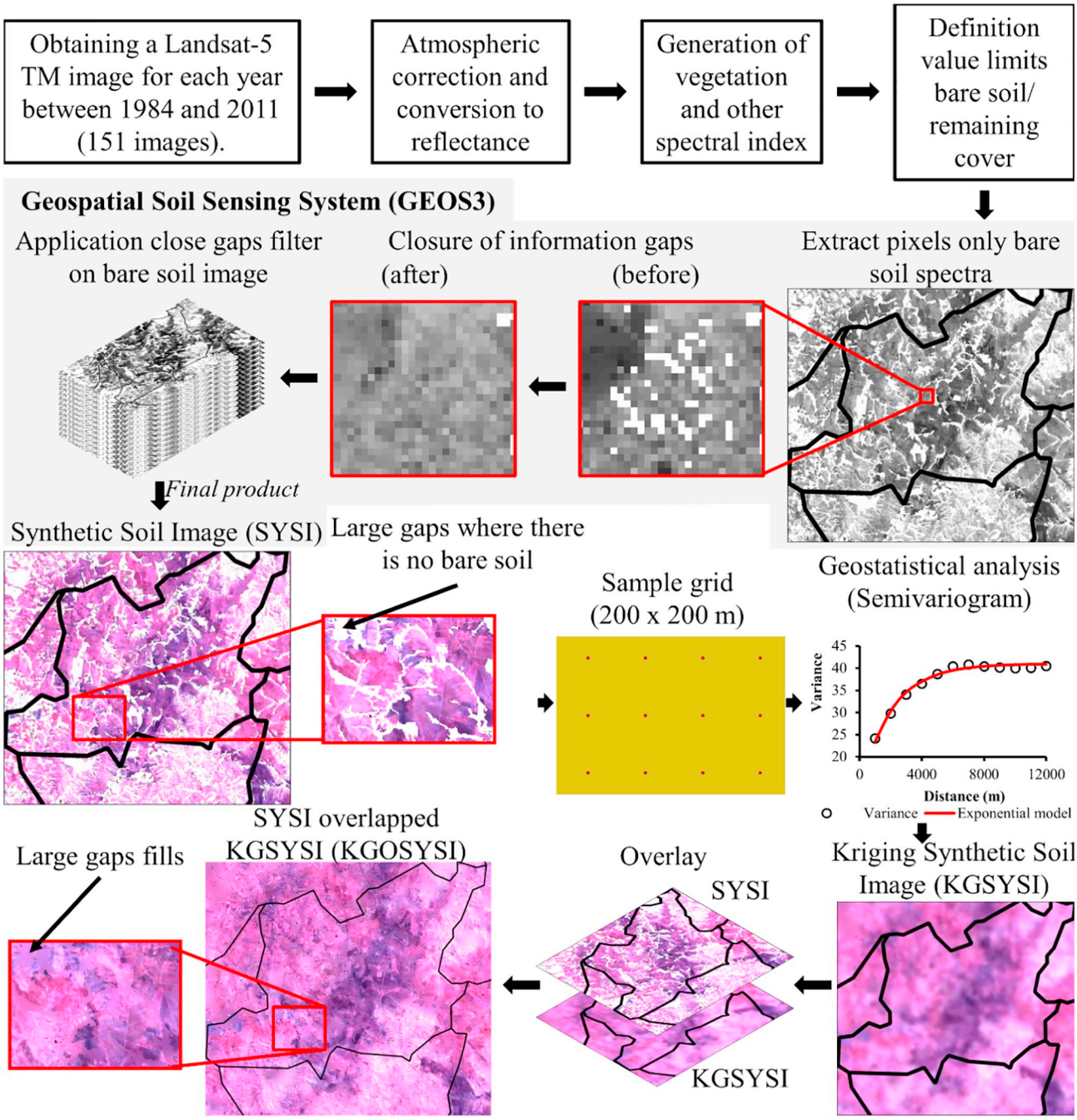

Fig. 2. Sequence of processing steps to generate bare soil composites for digital soil mapping. The Synthetic Soil Image (SYSI) is derived from the Geospatial Soil Sensing System (Demattê et al., 2018).

vii. Aluminum (Al): this is relevant to defining areas with high relative aluminum content (Al ≥ 4 cmolc kg^{-1}, CA ≥ 20 cmolc kg^{-1}, and m% ≥ 50 or V% < 50) and identifying Nitosols (dos Santos et al., 2013).

2.4. Calibration of multivariate models

The calibration of multivariate models was performed using the Geographically Weighted Regression (GWR) and Multiple Linear Regression (MLR) methods. These methods are included in the Spatial and Geostatistics package of SAGA GIS software, version 2.1.4 (Conrad et al., 2015). We have tested the MLR because it is the most common and simple method used for multivariate calibrations, although it does not consider spatial dependence. We also used GWR for comparative purposes since it accounts for spatial dependence.

MLR correlates a given attribute with multiple independent variables or covariates, which can be satellite image bands and/or relief attributes similar to those developed by Odeh et al. (2006). MLR can be represented by:

$$y_i = a_0 + \sum_k a_k x_{ik} + \varepsilon_i,$$

where y_i represents the predicted attribute at point i, a_k represents the multiplying coefficient related to independent variable x_{ik}, and ε_i is the error of the prediction estimation at point i (Fotheringham et al., 1998).

The GWR is an alternative to MLR, since it considers the position and spatial relationships among samples by determining distance weights, which are considered for the calibration (Fotheringham et al.,

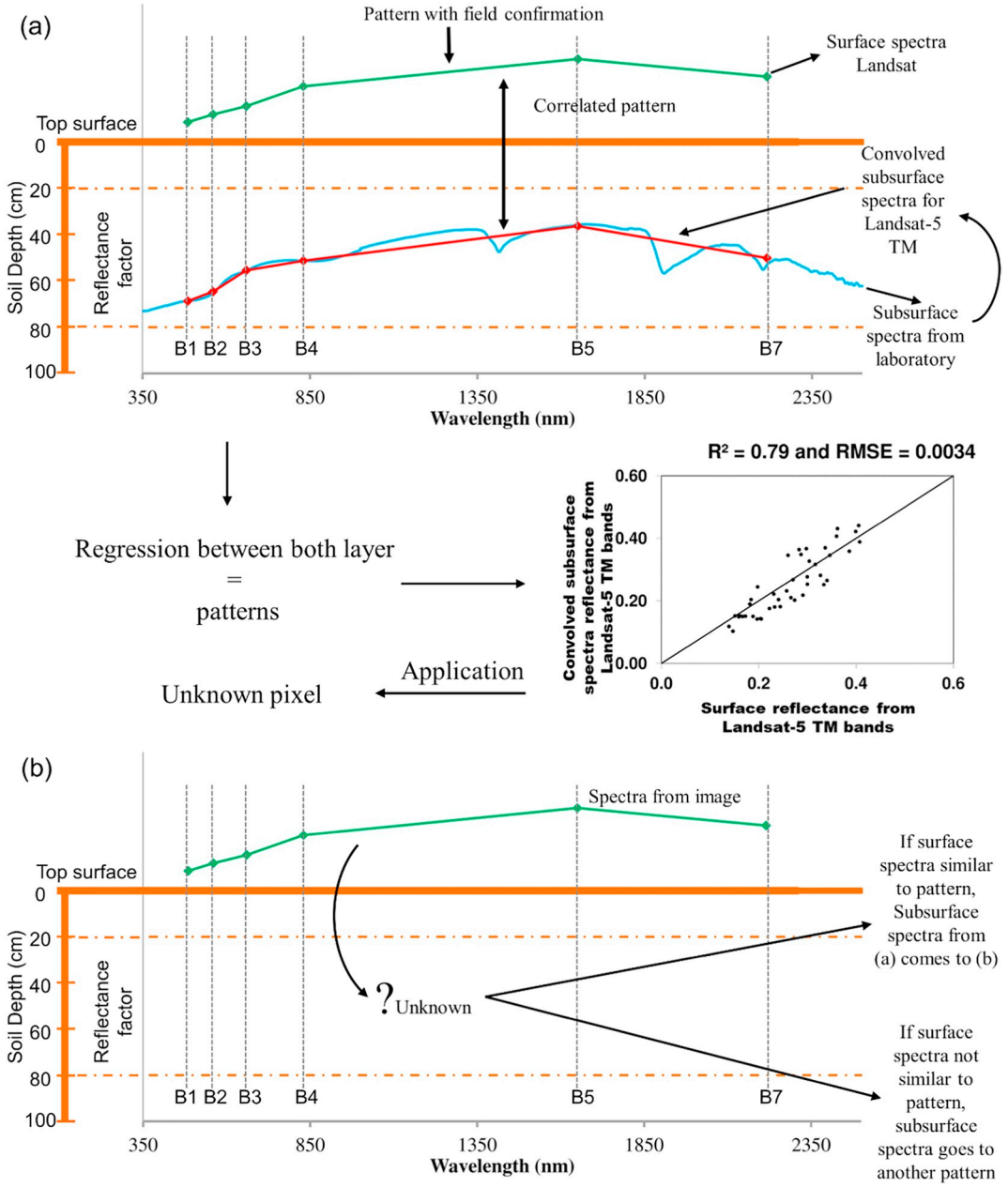

Fig. 3. Relationship between surface and subsurface spectral reflectance. Pattern with field confirmation (a); Unknown pattern of subsurface (b).

1998). Basically, the GWR equation is an extension of the MLR equation, with the added information of geographical location:

$$y_i = a_0 + \sum_k a_k(u_i, v_i)x_{ik} + \varepsilon_i,$$

where (u_i, v_i) represent the coordinates of point i in space, $a_k(u_i, v_i)$ is the geographically weighted continuous function $a_k(u, v)$ of point i, x_{ik} represents the independent variable k of point i, and ε_i is the error of the prediction estimate at point i (Fotheringham et al., 1998).

263 of the sampling points (80%) were used to calibrate the models and 65 points (20%) were chosen for the validation at random (Fig. 1). Subsequently, we spatialized the soil attributes using the GWR and MLR in the surface and subsurface layers by using the covariate layers.

2.5. Subsurface spectral reflectance

The laboratory spectra of the subsurface soil were convolved into the Landsat 5 Thematic Mapper (TM) spectral bands using a Gaussian function (Demattê et al., 2018). This step is performed by using a weighted average resampling approach, generating a multispectral dataset from the spectral data. Multispectral TM bands correspond to the visible, near infrared and shortwave infrared spectral regions: band 1 (450–520 nm); band 2 (520–600 nm); band 3 (630–690 nm); band 4 (760–900 nm); band 5 (1550–1750 nm) and; band 7 (2080–2350 nm).

Subsurface reflectance was estimated and spatialized from the association of the convolved laboratory spectra and the surface spectra of SYSI (Fig. 3a, Fig. 4). The results were the denominated Bare Subsurface Soil Image from both KGSYSI (BSSIKG) and KGOSYSI (BSSIKGO). The estimated subsurface spectral reflectance was tested as a covariate, in order to predict soil attributes at 80–100 cm depth. Furthermore, the ability of the surface reflectance of SYSI to estimate subsurface soil attributes was also tested, in addition to the spectral reflectance patterns of the subsurface (Fig. 3b).

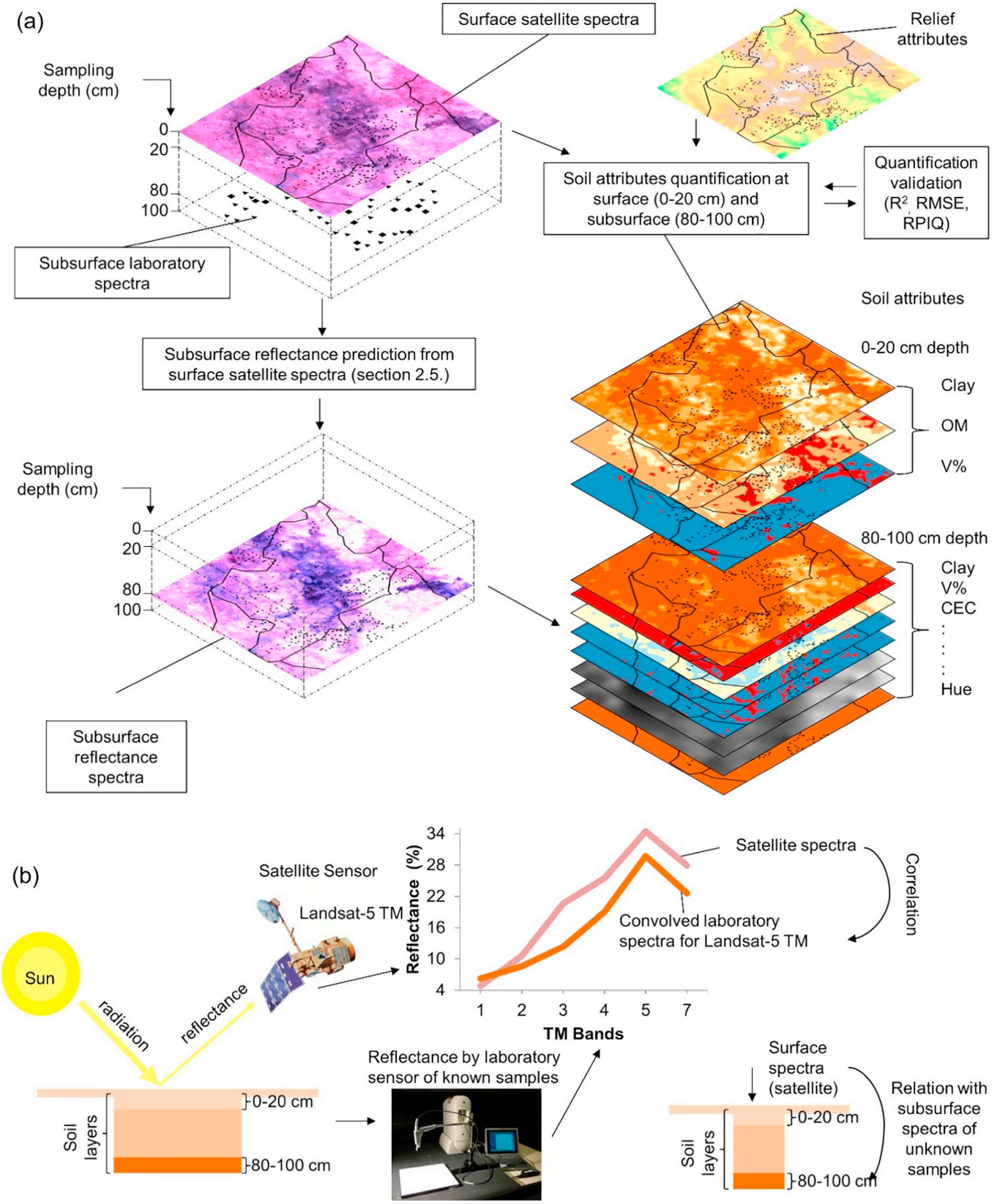

Fig. 4. Prediction of spectral reflectance of the subsurface layer and estimation of soil attributes at 0–20 and 80–100 cm layers (a). Workflow illustration of the steps and the relationship between surface spectral reflectance retrieved from satellite sensor and subsurface spectra acquired from the laboratory sensor (b).

Table 1
Prediction and validation of subsurface reflectance (80 to 100 cm) based on surface reflectance from satellite image data and multivariate statistical methods.

Subsurface band	Calibration method	Covariate source	Covariates (surface bands)	R^2_{adj}	RMSE	RPIQ
Band 1	GWR	KGOSYSI	Band2 + Band3 + Band4 + Band5	0.62	0.02	2.33
		KGSYSI		0.60	0.02	2.22
	MRL	KGOSYSI		0.46	0.03	1.96
		KGSYSI		0.44	0.03	1.92
Band 2	GWR	KGOSYSI	Band2 + Band3 + Band4 + Band5	0.72	0.03	2.70
		KGSYSI		0.66	0.03	2.45
	MRL	KGOSYSI		0.60	0.04	2.27
		KGSYSI		0.58	0.04	2.18
Band 3	GWR	KGOSYSI	Band2 + Band3 + Band4 + Band5 + Band7	0.69	0.04	2.35
		KGSYSI		0.64	0.05	2.20
	MRL	KGOSYSI		0.63	0.05	2.11
		KGSYSI		0.62	0.05	2.09
Band 4	GWR	KGOSYSI	Band3 + Band4 + Band5 + Band7	0.69	0.05	2.31
		KGSYSI		0.68	0.05	2.30
	MRL	KGOSYSI		0.61	0.07	1.90
		KGSYSI		0.58	0.06	1.94
Band 5	GWR	KGOSYSI	Band5 + Band7	0.65	0.12	1.67
		KGSYSI		0.69	0.11	1.77
	MRL	KGOSYSI		0.63	0.13	1.60
		KGSYSI		0.67	0.12	1.68
Band 7	GWR	KGOSYSI	Band5 + Band7	0.64	0.06	2.39
		KGSYSI		0.67	0.05	2.49
	MRL	KGOSYSI		0.64	0.06	2.34
		KGSYSI		0.66	0.06	2.47

MRL: Multiple linear regression; GWR: Geographically weighted regression; SYSI: Synthetic soil image; KGSYSI: SYSI generated by kriging estimates; KGOSYSI: SYSI generated by combining original SYSI and kriging estimates for only the non-filled gaps; R^2_{adj}: Adjusted coefficient of determination at 0.05 significance; RMSE: Root mean square error; RPIQ: Ratio of performance to interquartile range.

2.6. Soil attributes spatialization

Fig. 4 illustrates the workflow where soil attributes are predicted for two depths (two soil layers) with the addition of relief attributes as covariates. Based on model performance, the covariates selected for calibration with the GWR and MLR, varied for each soil attribute. For soil surface attributes, we tested the KGSYSI or KGOSYSI bands. For the subsurface layer, the covariates were primarily the subsurface estimates from both KGSYSI and KGOSYSI but, in some cases, surface reflectance was tested when the predictions outperformed the subsurface covariates. Additionally, for some subsurface attributes, terrain attributes were included in the calibration models. In Section 3, we present the best-performing associations of covariates for predicting and validating subsurface reflectance (80–100 cm) based on surface reflectance from satellite image data.

We refer to this process as the “Spectral Pedotransfer Function (SPEDO)”. The SPEDO consists of two principles: (i) the calibration of pedotransfer functions with synthetic soil images (SYSI), which are based on multitemporal satellite spectral reflectance (hence the term “Spectral” in SPEDO); and (ii) the application of the resulting products for digital soil mapping. When the spectral reflectance of the soil surface is retrieved, the subsurface layer data can be calibrated with surface information based on empirical relationships.

2.7. Validation of soil attribute estimates

Soil attributes from the surface and subsurface were validated for 20% of the samples (Fig. 1). We used the root mean-squared error (RMSE), the adjusted coefficient of determination (R^2_{adj}) and the ratio of performance to interquartile range (RPIQ) values (Bellon-Maurel et al., 2010) to compare all models and each soil attribute. High values of R^2_{adj} help to explain the predictors, whereas low values of RMSE denote good performance. The RPIQ values indicate the factors affecting prediction accuracy of non-available data (Keskin and Grunwald, 2018).

3. Results and discussion

3.1. Relationship between surface and subsurface spectral data

The GEOS3 retrieved 67.72% bare soil coverage in the study area from Landsat-5 TM multitemporal satellite images, the remaining 32.28% of the area being filled by kriging estimates (KGSYSI). Thus, bare soil spectra were generated to achieve 100% coverage and used to test the covariates for attributes mapping.

Surface soil information can be associated with subsurface data, allowing surface spectra to predict the subsurface when the patterns are established through calibration. This is the first step in determining properties from both layers (Fig. 3). The convolved subsurface of Landsat-5 TM bands presented strong results, reaching R^2_{adj} between 0.60 and 0.72 and RPIQ between 2.0 and 2.5 (Table 1). However, the convolved spectra of Band 1 (using MLR) was less reliable ($R^2_{adj} < 0.50$) and, overall, GWR was slightly better than MLR for the same covariates.

Prediction of the subsurface convolved spectra of Band 1, Band 2, Band 3, and Band 4 from Landsat-5 TM was better using independent variables from KGOSYSI, while prediction of Band 5 and Band 7 was better when using independent variables from KGSYSI (Table 1). There have been many studies that have used laboratory and hyperspectral (Ließ et al., 2012; Nanni and Demattê, 2006; Ogen et al., 2017; Regmi and Rasmussen, 2018; Rizzo et al., 2016; Stevens et al., 2008) to assess the subsurface soil properties. These studies are based on field observations of surface and subsurface soil data. However, there is scarce information on subsurface reflectance prediction from surface information, as is proposed here.

3.2. Spatialization of soil attributes

The prediction of surface clay content by satellite spectra resulted in an R^2_{adj} between 0.50 and 0.75 with an RPIQ between 2.0 and 2.5, with the best independent variables being Bands 7, 5, 4, 3 and 2 (Table 2). In this case, multispectral bands from KGSYSI performed better than KGOSYSI. Comparing GWR with MLR as a predictive method for clay

Table 2
Prediction of surface soil attributes (0 to 20 cm) by multivariate statistical methods.

Soil attribute	Calibration method	Covariate source	Covariates (surface bands)	R^2_{adj}	RMSE	RPIQ
Clay1 (g kg^{-1})	GWR	KGSYSI	Band2 + Band3 + Band4 + Band5 + Band7	0.62	82.87	2.25
Clay2 (g kg^{-1})		KGOSYSI		0.53	91.88	2.03
Clay3 (g kg^{-1})	MRL	KGSYSI		0.54	91.54	2.04
Clay4 (g kg^{-1})		KGOSYSI		0.56	88.83	2.10
O.M. (g kg^{-1})	GWR	KGSYSI	Clay1 + Band7	0.38	7.13	1.96
		KGOSYSI	Clay2 + Band7	0.29	7.41	1.89
	MRL	KGSYSI	Clay3 + Band7	0.25	7.68	1.82
		KGOSYSI	Clay4 + Band7	0.21	7.81	1.79
V%	GWR	KGSYSI	Band2 + Band3 + Band4 + Band5	0.31	14.83	1.62
		KGOSYSI		0.30	14.95	1.61
	MRL	KGSYSI		0.20	16.04	1.50
		KGOSYSI		0.24	15.82	1.52

MRL: Multiple linear regression; GWR: Geographically weighted regression; SYSI: Synthetic soil image; KGSYSI: SYSI generated by kriging estimates; KGOSYSI: SYSI generated by combining original SYSI and kriging estimates for only the non-filled gaps; R^2_{adj}: Adjusted coefficient of determination at 0.05 significance; RMSE: Root mean square error; RPIQ: Ratio of performance to interquartile range.

estimation, GWR presented a better performance. This is evidence of the importance of considering spatial relationships between sampling locations for predictive purposes.

The results obtained for surface clay are in agreement with Steinberg et al. (2016) using an airborne hyperspectral sensor (by PLSR). It is also in agreement with Shabou et al. (2015), where R^2_{adj} of 0.65 for Landsat-5 TM (Band 5 and Band 7 index). The soil surface chemical attributes, such as organic matter (OM) and base saturation (V %), presented unreliable results ($R^2_{adj} < 0.50$ and RPIQ between 1.5 and 2.0, see Table 2). Low R^2_{adj} values for these attributes were also observed by Bhering et al. (2016). However, low RMSE values were achieved and the prediction were used to separate eutrophic/dystrophic (V% = 50) and organosols (OM > 13%). Comparing GWR with MLR, a relative superiority of GWR was observed in the predictions (Table 2).

The improved prediction performance of independent variables using KGSYSI bands can be explained by the smooth transitions of the reflectance values (Fig. 5, RGB 543 composite), whereas KGOSYSI presented more abrupt transitions (Fig. 5). These transitions occur due to multitemporal variances in reflectance, which may occur due to the presence of noise and are not naturally representative of the spatial changes of the soil attributes. The kriging smoothing effect, as reported by da Rocha et al. (2007), can correct some of these multitemporal variations, as it overestimates values near to the minimum values and underestimates values near to the maximum values. However, it can also impact the spatial predictions (Yamamoto, 2005).

In relation to the subsurface soil attributes, clay presented good estimates (Table 3), which were in agreement with Steinberg et al. (2016). Among the independent variables and prediction methods, the best result was for KGSYSI using GWR ($R^2_{adj} = 0.63$). In this case, surface spectral information presented a higher correlation with subsurface clay. This can be explained by the similar spectral signatures along a profile of the same soil class, as observed by Ben-Dor et al. (2008) and Araújo et al. (2015). Estimating clay content by the MLR method from KGOSYSI was unreliable ($R^2_{adj} < 0.50$). The predictions also presented low values ($R^2_{adj} < 0.50$ and RPIQ < 2.0) for chemical attributes (Al, V%, m% and CEC, see Table 2). For the prediction of these attributes, the GWR method was superior to MLR (Table 3).

Hue estimates were obtained with R^2_{adj} of 0.57 and RPIQ of 2.07, while value and chroma with R^2_{adj} of 0.74 (RIPQ = 3.04) and R^2_{adj} of

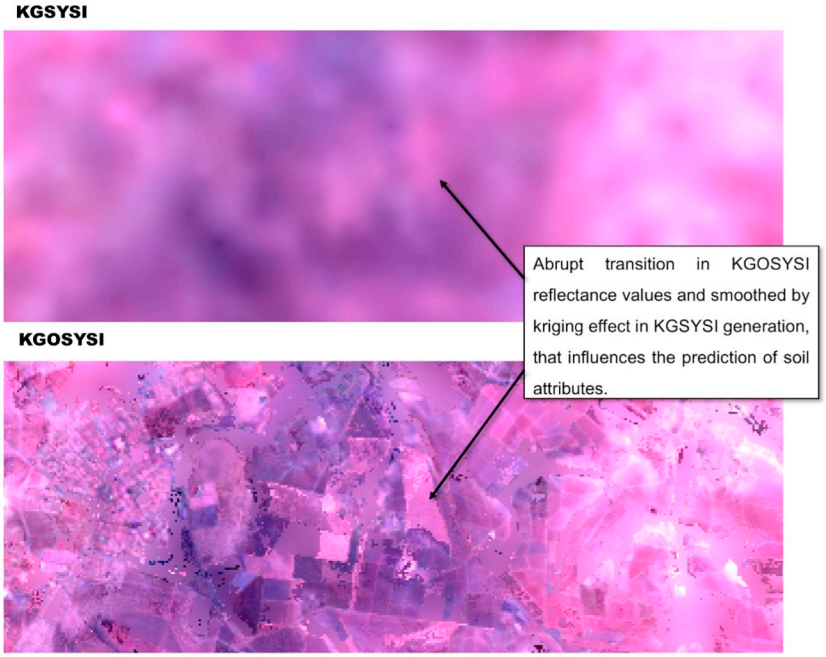

Fig. 5. Subset of the KGSYSI and KGOSYSI to demonstrate transitional patterns of surface reflectance values (false-color composite RGB 543). SYSI: Synthetic Soil Image; KGSYSI: SYSI generated by kriging estimates; KGOSYSI: SYSI generated by combining original SYSI and kriging estimates only for the non-filled gaps.

Table 3
Prediction of subsurface soil attributes (80 to 100 cm) by multivariate statistical methods.

Soil attribute	Prediction method	Covariates source	Covariates	R^2_{adj}	RMSE	RPIQ
Clay1 (g kg^{-1})	GWR	KGSYSI	Band7, Band5, and Band4	0.63	88.24	2.68
Clay2 (g kg^{-1})		KGOSYSI		0.54	101.43	2.33
Clay3 (g kg^{-1})	MRL	KGSYSI		0.55	97.66	2.42
Clay4 (g kg^{-1})		KGOSYSI		0.43	112.85	2.09
V%1	GWR	KGSYSI and terrain attributes	TPI, SLH, VLD, SAR, Band7, and Band4	0.12	20.42	1.75
V%2		KGOSYSI and terrain attributes		0.14	20.19	1.77
V%3	MRL	KGSYSI and terrain attributes		0.05	21.09	1.70
V%4		KGOSYSI and terrain attributes		0.07	20.85	1.71
CEC1 (mmolc/dm^3)	GWR	Subsurface spectra from KGSYSI	Band5, Band7, and Clay1	0.35	69.82	0.89
CEC2 (mmolc/dm^3)		Subsurface spectra from KGOSYSI	Band5, Band7, and Clay2	0.29	71.73	0.87
CEC3 (mmolc/dm^3)	GWR	Subsurface spectra from KGSYSI	Band5, Band7, and Clay3	0.06	83.26	0.75
CEC4 (mmolc/dm^3)		Subsurface spectra from KGOSYSI	Band5, Band7, and Clay4	0.02	84.37	0.74
m%1	GWR	Subsurface spectra from KGSYSI	Band7, Band5, Band4, and V%1	0.27	17.01	1.35
m%2		Subsurface spectra from KGOSYSI	Band7, Band5, Band4, and V%2	0.23	17.47	1.32
m%3	MRL	Subsurface spectra from KGSYSI	Band7, Band5, Band4, and V%3	0.11	19.16	1.20
m%4		Subsurface spectra from KGOSYSI	Band7, Band5, Band4, and V%4	0.17	18.31	1.26
Al (mmolc/dm^3)	GWR	Subsurface spectra from KGSYSI	CEC1, V%1, and m%1	0.32	11.95	1.51
		Subsurface spectra from KGOSYSI	CEC2 V%2, and m%2	0.21	13.22	1.36
	MRL	Subsurface spectra from KGSYSI	CEC3, V%3, and m%3	0.36	11.73	1.53
		Subsurface spectra from KGOSYSI	CEC4, V%4, and m%4	0.07	14.56	1.24
Chroma	GWR	Subsurface spectra from KGOSYSI	Band1, Band2, and Band3	0.63	0.52	2.78
		Subsurface spectra from KGSYSI		0.43	0.65	2.24
	MRL	Subsurface spectra from KGOSYSI		0.67	0.51	2.87
		Subsurface spectra from KGSYSI		0.34	0.69	2.09
Hue	GWR	Subsurface spectra from KGOSYSI	Band1, Band2, Band3, and Band4	0.57	1.28	2.07
		Subsurface spectra from KGSYSI		0.49	1.40	1.90
	MRL	Subsurface spectra from KGOSYSI		0.45	1.43	1.86
		Subsurface spectra from KGSYSI		0.30	1.60	1.66
Value	GWR	Subsurface spectra from KGOSYSI	Band1, Band2, Band3	0.73	0.26	2.96
		Subsurface spectra from KGSYSI		0.64	0.30	2.59
	MRL	Subsurface spectra from KGOSYSI		0.74	0.25	3.04
		Subsurface spectra from KGSYSI		0.60	0.32	2.45

TPI: Topographic position index; SLH: Slope Height; VLD: Valley Depth; SAR: Surface Area; MRL: Multiple linear regression; GWR: Geographically weighted regression; SYSI: Synthetic soil image; KGSYSI: SYSI generated by kriging estimates; KGOSYSI: SYSI generated by combining original SYSI and kriging estimates for only the non-filled gaps; R^2_{adj}: Adjusted coefficient of determination at 0.05 significance; RMSE: Root mean square error; RPIQ: Ratio of performance to interquartile range.

0.67 (RPIQ = 2.87), respectively (Table 3). These results are in agreement with the correlations between reflectance and the Munsell color system observed by Escadafal et al. (1989), Mathieu et al. (1998), and Post et al. (1994). These authors correlated the Munsell color with satellite images, whereas Viscarra Rossel and Behrens (2010) correlated laboratory spectra with the Munsell color. GWR presented the best performance for hue prediction, being slightly lower than the MLR/KGOSYSI2 combination for value and chroma (Table 3). These results show that the correlation of these attributes with the spectral values is relevant to prediction.

Hue, value, and chroma predictions achieved the best results by using KGOSYSI (Table 3), while predictions of clay content, CEC, m%, V %, and Al were better with KGSYSI (Tables 2 and 3). In this case (and different from previous observations), the multitemporal variation of reflectance for the visible bands (Band 1, Band 2, and Band 3) used in the iron and color precision, is smaller than in the infrared bands. The Kriging smoothing effect overestimated minimum locations and underestimated maximum locations, influencing this distinction.

Several studies (Dewitte et al., 2012; Dobos et al., 2000; Dwivedi, 2001) have reported that spectral data obtained by onboard satellite sensors can differentiate many pedological classes, although they only detect the soil surface layer. Nanni et al. (2014) also demonstrated that satellite images can be used to discriminate soil classes which is related to subsurface patterns. Zeng et al. (2016) observed that surface information can be inferred from subsurface information. These reports agree with the results of this study, i.e. that surface reflectance can be used as a strategy for inferring the subsurface, with R^2_{adj} above 0.50 (Tables 2 and 3). Quantification of soil attributes by the spectra generated in the laboratory is nothing new. Soriano-Disla et al. (2014) and Nocita et al. (2015) have demonstrated this and Viscarra Rossel et al. (2016a, 2016b) conclude that some soil properties have a high association with laboratory spectra. Thus, the literature corroborates our findings on the quantification of soil attributes, even though their studies were conducted using only laboratory spectra.

Remote sensing is now widely used. Indeed, only the top 3 cm of the surface can be detected by these optical sensors. Pedotransfer functions (McBratney et al., 2002) are defined as predictive tools based on certain soil attribute patterns relative to another, allowing the transfer of soil information from known to unknown locations. This concept has been widely used to map soil attributes and classes (Behrens et al., 2010; Finke, 2012; Hartemink and Minasny, 2014; Michéli et al., 2016). By using the SPEDO function, we have demonstrated that it is possible to use surface spectral information to predict subsurface spectra and, following on from that, the function can be applied to map soil attributes and classes.

4. Conclusion

Based on satellite surface spectral information, subsurface soil properties were successfully estimated (i.e. clay content, hue and value) with $0.61 < R^2_{adj} < 0.70$, by using spectral pedotransfer functions (SPEDO). The spectral reflectance of soil surfaces, obtained by satellite sensors, correlated with the subsurface spectra, reaching R^2_{adj} of 0.72. This supported the spatial prediction of subsurface spectra based on the surface patterns and mapping of soil attributes by digital soil mapping. The results indicate the existence of a strong relationship between surface soil characteristics (patterns) that allow the inference of subsurface features, with a certain margin of error. Overall, geographically weighted regression provided better estimations of soil attributes than the multivariate linear regression. Last but not least, we strongly

believe that the SPEDO will open up new opportunities for obtaining information about subsurface soils, based on satellite data, in order to assist with digital soil mapping. Despite this important achievement, the prediction of soil subsurface properties is still a task that requires continuous research to aggregate other upcoming techniques.

Acknowledgements

This research is part of master's dissertation of the second author, presented to the Graduate Program of Soil and Plant Nutrition at the "Luiz de Queiroz" College of Agriculture, University of São Paulo. We acknowledge the financial support of the São Paulo Research Foundation (FAPESP grant numbers 2014/22262-0, 2016/26124-6 and 2016/01597-9) and the National Council for Scientific and Technological Development (CNPq). Also, this study was financed in part by the Coordenação de Aperfeiçoamento de Pessoal de Nível Superior - Brasil (CAPES) - Finance Code 001. We also thank members of the Geotechnologies in Soil Science Group (GeoCIS/GeoSS) (http://esalqgeocis.wixsite.com/geocis).

References

Agbu, P.A., Fehrenbacher, D.J., Jansen, I.J., 1990. Soil property relationships with SPOT satellite digital data in East Central Illinois. Soil Sci. Soc. Am. J. 54, 807. https://doi.org/10.2136/sssaj1990.03615995005400030031x.

Araújo, S.R., Söderström, M., Eriksson, J., Isendahl, C., Stenborg, P., Demattê, J.M., 2015. Determining soil properties in Amazonian Dark Earths by reflectance spectroscopy. Geoderma 237–238, 308–317. https://doi.org/10.1016/j.geoderma.2014.09.014.

Behrens, T., Zhu, A.-X., Schmidt, K., Scholten, T., 2010. Multi-scale digital terrain analysis and feature selection for digital soil mapping. Geoderma 155, 175–185. https://doi.org/10.1016/j.geoderma.2009.07.010.

Bellon-Maurel, V., Fernandez-Ahumada, E., Palagos, B., Roger, J.-M., McBratney, A., 2010. Critical review of chemometric indicators commonly used for assessing the quality of the prediction of soil attributes by {NIR} spectroscopy. TrAC Trends Anal. Chem. 29, 1073–1081. https://doi.org/10.1016/j.trac.2010.05.006.

Ben-Dor, E., Heller, D., Chudnovsky, A., 2008. A novel method of classifying soil profiles in the field using optical means. Soil Sci. Soc. Am. J. 72, 1113. https://doi.org/10.2136/sssaj2006.0059.

Bhering, S.B., Chagas, C.da S., Carvalho Junior, W.de, Pereira, N.R., Calderano Filho, B., Pinheiro, H.S.K., 2016. Mapeamento digital de areia, argila e carbono orgânico por modelos Random Forest sob diferentes resoluções espaciais. Pesqui. Agropecuária Bras 51, 1359–1370. https://doi.org/10.1590/s0100-204x2016000900035.

Bockheim, J.G., Gennadiyev, A.N., Hartemink, A.E., Brevik, E.C., 2014. Soil-forming factors and soil taxonomy. Geoderma 226–227, 231–237. https://doi.org/10.1016/j.geoderma.2014.02.016.

Conrad, O., Bechtel, B., Bock, M., Dietrich, H., Fischer, E., Gerlitz, L., Wehberg, J., Wichmann, V., Böhner, J., 2015. System for automated geoscientific analyses (SAGA) v. 2.1.4. Geosci. Model Dev. 8, 1991–2007. https://doi.org/10.5194/gmd-8-1991-2015.

da Rocha, M.M., Lourenço, D.A., Leite, C.B.B., 2007. Aplicação de krigagem com correção do efeito de suavização em dados de potenciometria da cidade de Pereira Barreto. In: SP. Geol. USP. Série Científica. 7. pp. 37–48. https://doi.org/10.5327/Z1519-874X2007000200003.

Demattê, J.A.M., Alves, M.R., Terra, F. da S., Bosquilia, R.W.D., Fongaro, C.T., Barros, P.P. da S., 2016. Is it possible to classify topsoil texture using a sensor located 800 km away from the surface? Rev. Bras. Ciênc. Solo 40. https://doi.org/10.1590/18069657rbcs20150335.

Demattê, J.A.M., Fiorio, P.R., Ben-Dor, E., 2009. Estimation of soil properties by orbital and laboratory reflectance means and its relation with soil classification. Open Remote Sens. J. 2, 12–23.

Demattê, J.A.M., Fongaro, C.T., Rizzo, R., Safanelli, J.L., 2018. Geospatial soil sensing system (GEOS3): a powerful data mining procedure to retrieve soil spectral reflectance from satellite images. Remote Sens. Environ. 212, 161–175. https://doi.org/10.1016/j.rse.2018.04.047.

Dewitte, O., Jones, A., Elbelrhiti, H., Horion, S., Montanarella, L., 2012. Satellite remote sensing for soil mapping in Africa: an overview. Prog. Phys. Geogr. 36, 514–538. https://doi.org/10.1177/0309133312446981.

Diek, S., Fornallaz, F., Schaepman, M.E., de Jong, R., 2017. Barest pixel composite for agricultural areas using landsat time series. Remote Sens. 9, 1245. https://doi.org/10.3390/rs9121245.

Dobos, E., Micheli, E., Baumgardner, M.F., Biehl, L., Helt, T., 2000. Use of combined digital elevation model and satellite radiometric data for regional soil mapping. Geoderma 97, 367–391. https://doi.org/10.1016/S0016-7061(00)00046-X.

Donagemma, G.K., de Campos, D.V.B., Calderano, S.B., Teixeira, W.G., Viana, J.H.M., 2011. Manual de métodos de análise de solo, 2 rev. Embrapa Solos.

dos Santos, H.G., Jacomine, P.K.T., dos Anjos, L.H.C., de Oliveira, V.Á., Lumbreras, J.F., Coelho, M.R., de Almeida, J.A., Cunha, T.J.F., de Oliveira, J.B., 2013. Sistema brasileiro de classificação de solos, 3 ed. rev. EMBRAPA, Brasília, DF.

Dwivedi, R.S., 2001. Soil resources mapping: a remote sensing perspective. Remote Sens. Rev. 20, 89–122. https://doi.org/10.1080/02757250109532430.

Escadafal, R., Girard, M.-C., Courault, D., 1989. Munsell soil color and soil reflectance in the visible spectral bands of landsat MSS and TM data. Remote Sens. Environ. 27, 37–46. https://doi.org/10.1016/0034-4257(89)90035-7.

Finke, P.A., 2012. On digital soil assessment with models and the Pedometrics agenda. Geoderma 171–172, 3–15. https://doi.org/10.1016/j.geoderma.2011.01.001.

Fotheringham, A.S., Charlton, M.E., Brunsdon, C., 1998. Geographically weighted regression: a natural evolution of the expansion method for spatial data analysis. Environ. Plan. A 30, 1905–1927. https://doi.org/10.1068/a301905.

Franceschini, M.H.D., Demattê, J.A.M., da Silva Terra, F., Vicente, L.E., Bartholomeus, H., de Souza Filho, C.R., 2015. Prediction of soil properties using imaging spectroscopy: considering fractional vegetation cover to improve accuracy. Int. J. Appl. Earth Obs. Geoinf. 38, 358–370. https://doi.org/10.1016/j.jag.2015.01.019.

Galvão, L., Vitorello, I., Formaggio, A.R., 1997. Relationships of spectral reflectance and color among surface and subsurface horizons of tropical soil profiles. Remote Sens. Environ. 61, 24–33. https://doi.org/10.1016/S0034-4257(96)00219-2.

Gerighausen, H., Menz, G., Kaufmann, H., 2012. Spatially explicit estimation of clay and organic carbon content in agricultural soils using multi-annual imaging spectroscopy data. Appl. Environ. Soil Sci. 2012, 1–23. https://doi.org/10.1155/2012/868090.

Grunwald, S., 2010. Current state of digital soil mapping and what is next. In: Digital Soil Mapping. Springer Netherlands, Dordrecht, pp. 3–12. https://doi.org/10.1007/978-90-481-8863-5_1.

Hartemink, A.E., Minasny, B., 2014. Towards digital soil morphometrics. Geoderma 230–231, 305–317. https://doi.org/10.1016/j.geoderma.2014.03.008.

IUSS Working Group WRB, 2015. World Reference Base for Soil Resources 2014, Update 2015. International Soil Classification System for Naming Soils and Creating Legends for Soil Maps. World Soil Resources Reports No. 106. FAO, Rome.

Jenny, H., 1941. Factors of Soil Formation - a System of Quantitative Pedology. McGraw-Hill, New York.

Keskin, H., Grunwald, S., 2018. Regression kriging as a workhorse in the digital soil mapper's toolbox. Geoderma 326, 22–41. https://doi.org/10.1016/j.geoderma.2018.04.004.

Khayamim, F., Wetterlind, J., Khademi, H., Robertson, A.H.J., Cano, A.F., Stenberg, B., 2015. Using visible and near infrared spectroscopy to estimate carbonates and gypsum in soils in arid and subhumid regions of Isfahan, Iran. J. Near Infrared Spectrosc. 23, 155–165. https://doi.org/10.1255/jnirs.1157.

Ließ, M., Glaser, B., Huwe, B., 2012. Uncertainty in the spatial prediction of soil texture. Geoderma 170, 70–79. https://doi.org/10.1016/j.geoderma.2011.10.010.

Mathieu, R., Pouget, M., Cervelle, B., Escadafal, R., 1998. Relationships between satellite-based radiometric indices simulated using laboratory reflectance data and typic soil color of an arid environment. Remote Sens. Environ. 66, 17–28. https://doi.org/10.1016/S0034-4257(98)00030-3.

McBratney, A., Mendonça Santos, M., Minasny, B., 2003. On digital soil mapping. Geoderma 117, 3–52. https://doi.org/10.1016/S0016-7061(03)00223-4.

McBratney, A.B., Minasny, B., Cattle, S.R., Vervoort, R.W., 2002. From pedotransfer functions to soil inference systems. Geoderma 109, 41–73. https://doi.org/10.1016/S0016-7061(02)00139-8.

Mezzalira, S., 1966. Folha geológica de Piracicaba SF23-M 300. Instituto Geográfico e geológico do Estado de São Paulo.

Michéli, E., Láng, V., Owens, P.R., McBratney, A., Hempel, J., 2016. Testing the pedometric evaluation of taxonomic units on soil taxonomy — a step in advancing towards a universal soil classification system. Geoderma 264, 340–349. https://doi.org/10.1016/j.geoderma.2015.09.008.

Miller, B.A., Schaetzl, R.J., 2016. History of soil geography in the context of scale. Geoderma 264, 284–300. https://doi.org/10.1016/j.geoderma.2015.08.041.

Moore, I.D., Gessler, P.E., Nielsen, G.A., Peterson, G.A., 1993. Soil attribute prediction using terrain analysis. Soil Sci. Soc. Am. J. 57, NP. https://doi.org/10.2136/sssaj1993.572NPb.

Mulder, V.L., de Bruin, S., Schaepman, M.E., Mayr, T.R., 2011. The use of remote sensing in soil and terrain mapping — a review. Geoderma 162, 1–19. https://doi.org/10.1016/j.geoderma.2010.12.018.

Nanni, M.R., Demattê, J.A.M., 2006. Spectral reflectance methodology in comparison to traditional soil analysis. Soil Sci. Soc. Am. J. 70, 393–407. https://doi.org/10.2136/SSSAJ2003.0285.

Nanni, M.R., Demattе, J.A.M., Junior, C.A. da S., Romagnoli, F., da Silva, A.A., Cezar, E., Gasparotto, A. de C., 2014. Soil mapping by laboratory and orbital spectral sensing compared with a traditional method in a detailed level. J. Agron. 13, 100–109. https://doi.org/10.3923/ja.2014.100.109.

Nocita, M., Stevens, A., van Wesemael, B., Aitkenhead, M., Bachmann, M., Barthès, B., Ben Dor, E., Brown, D.J., Clairotte, M., Csorba, A., Dardenne, P., Demattê, J.A.M., Genot, V., Guerrero, C., Knadel, M., Montanarella, L., Noon, C., Ramirez-Lopez, L., Robertson, J., Sakai, H., Soriano-Disla, J.M., Shepherd, K.D., Stenberg, B., Towett, E.K., Vargas, R., Wetterlind, J., 2015. Soil spectroscopy: an alternative to wet chemistry for soil monitoring. Adv. Agron. 132, 139–159. https://doi.org/10.1016/BS.AGRON.2015.02.002.

Odeh, I.O.A., Crawford, M., McBratney, A.B., 2006. Digital Mapping of soil Attributes for Regional and Catchment Modelling, Using Ancillary Covariates, Statistical and Geostatistical Techniques. pp. 437–622. https://doi.org/10.1016/S0166-2481(06)31032-X.

Ogen, Y., Goldshleger, N., Ben-Dor, E., 2017. 3D spectral analysis in the VNIR–SWIR spectral region as a tool for soil classification. Geoderma 302, 100–110. https://doi.org/10.1016/j.geoderma.2017.04.020.

Ordóñez, R.A., Castellano, M.J., Hatfield, J.L., Helmers, M.J., Licht, M.A., Liebman, M., Dietzel, R., Martinez-Feria, R., Iqbal, J., Puntel, L.A., Córdova, S.C., Togliatti, K., Wright, E.E., Archontoulis, S.V., 2018. Maize and soybean root front velocity and maximum depth in Iowa, USA. Field Crop Res. 215, 122–131. https://doi.org/10.

1016/j.fcr.2017.09.003.
Polidoro, J.C., Mendonça-Santos, M.D.L., Lumbreras, J.F., Coelho, M.R., Filho, Carvalho, De, A., Da Motta, P.E.F., Junior, Carvalho, De, W., Filho, Araujo, De, J.C., Curcio, G.R., Correia, J.R., Martins, E.D.S., Spera, S.T., Oliveira, S.R.D.M., Bolfe, E.L., Manzatto, C.V., Tosto, S.G., Venturieri, A., Sa, I.B., De Oliveira, V.A., Shinzato, E., Anjos, L.H.C. Dos, Valladares, G.S., Ribeiro, J.L., De Medeiros, P.S.C., Moreira, F.M.D.S., Silva, L.S.L., Sequinatto, L., Aglio, M.L.D., Dart, R.D.O., 2016. Programa Nacional de Solos do Brasil (PronaSolos), 1o ed. Embrapa Solos, Rio de Janeiro, RJ.
Post, D.F., Lucas, W.M., White, S.A., Ehasz, M.J., Batchily, A.K., Horvath, E.H., 1994. Relations between soil color and Landsat reflectance on semiarid rangelands. Soil Sci. Soc. Am. J. 58, 1809. https://doi.org/10.2136/sssaj1994.03615995005800060033x.
Regmi, N.R., Rasmussen, C., 2018. Predictive mapping of soil-landscape relationships in the arid Southwest United States. Catena 165, 473–486. https://doi.org/10.1016/j.catena.2018.02.031.
Rizzo, R., Demattê, J.A.M., Lepsch, I.F., Gallo, B.C., Fongaro, C.T., 2016. Digital soil mapping at local scale using a multi-depth Vis–NIR spectral library and terrain attributes. Geoderma 274, 18–27. https://doi.org/10.1016/j.geoderma.2016.03.019.
Shabou, M., Mougenot, B., Chabaane, Z., Walter, C., Boulet, G., Aissa, N., Zribi, M., 2015. Soil clay content mapping using a time series of Landsat TM data in semi-arid lands. Remote Sens. 7, 6059–6078. https://doi.org/10.3390/rs70506059.
Soil Survey Staff, 2014. Soil taxonomy: a basic system of soil classification for making and interpreting soil surveys. In: Natural Resources Conservation Service. U.S. Department of Agriculture Handbook, Twelfth ed. .
Soriano-Disla, J.M., Janik, L.J., Viscarra Rossel, R.A., MacDonald, L.M., McLaughlin, M.J., 2014. The performance of visible, near-, and mid-infrared reflectance spectroscopy for prediction of soil physical, chemical, and biological properties. Appl. Spectrosc. Rev. 49, 139–186. https://doi.org/10.1080/05704928.2013.811081.
Steinberg, A., Chabrillat, S., Stevens, A., Segl, K., Foerster, S., 2016. Prediction of common surface soil properties based on Vis-NIR airborne and simulated EnMAP imaging spectroscopy data: prediction accuracy and influence of spatial resolution. Remote Sens. 8, 613. https://doi.org/10.3390/rs8070613.
Stevens, A., van Wesemael, B., Bartholomeus, H., Rosillon, D., Tychon, B., Ben-Dor, E., 2008. Laboratory, field and airborne spectroscopy for monitoring organic carbon content in agricultural soils. Geoderma 144, 395–404. https://doi.org/10.1016/J.GEODERMA.2007.12.009.
Terra, F.S., Demattê, J.A.M., Viscarra Rossel, R.A., 2015. Spectral libraries for quantitative analyses of tropical Brazilian soils: comparing vis–NIR and mid-IR reflectance data. Geoderma 255–256, 81–93. https://doi.org/10.1016/j.geoderma.2015.04.017.
Vasques, G.M., Coelho, M.R., Dart, R.O., Oliveira, R.P., Teixeira, W.G., 2016. Mapping soil carbon, particle-size fractions, and water retention in tropical dry forest in Brazil. Pesq. Agrop. Brasileira 51, 1371–1385. https://doi.org/10.1590/s0100-204x2016000900036.
Viscarra Rossel, R.A.A., Behrens, T., 2010. Using data mining to model and interpret soil diffuse reflectance spectra. In: Geoderma, Diffuse Reflectance Spectroscopy in Soil Science and Land Resource Assessment. 158. pp. 46–54. https://doi.org/10.1016/j.geoderma.2009.12.025.
Viscarra Rossel, R.A., Behrens, T., Ben-Dor, E., Brown, D.J., Demattê, J.A.M., Shepherd, K.D., Shi, Z., Stenberg, B., Stevens, A., Adamchuk, V., Aïchi, H., Barthès, B.G., Bartholomeus, H.M., Bayer, A.D., Bernoux, M., Böttcher, K., Brodský, L., Du, C.W., Chappell, A., Fouad, Y., Genot, V., Gomez, C., Grunwald, S., Gubler, A., Guerrero, C., Hedley, C.B., Knadel, M., Morrás, H.J.M., Nocita, M., Ramirez-Lopez, L., Roudier, P., Campos, E.M.R., Sanborn, P., Sellitto, V.M., Sudduth, K.A., Rawlins, B.G., Walter, C., Winowiecki, L.A., Hong, S.Y., Ji, W., 2016a. A global spectral library to characterize the world's soil. Earth-Sci. Rev. 155, 198–230. https://doi.org/10.1016/j.earscirev.2016.01.012.
Viscarra Rossel, R.A., Behrens, T., Ben-Dor, E., Brown, D.J., Demattê, J.A.M., Shepherd, K.D., Shi, Z., Stenberg, B., Stevens, A., Adamchuk, V., Aïchi, H., Barthès, B.G., Bartholomeus, H.M., Bayer, A.D., Bernoux, M., Böttcher, K., Brodský, L., Du, C.W., Chappell, A., Fouad, Y., Genot, V., Gomez, C., Grunwald, S., Gubler, A., Guerrero, C., Hedley, C.B., Knadel, M., Morrás, H.J.M., Nocita, M., Ramirez-Lopez, L., Roudier, P., Campos, E.M.R., Sanborn, P., Sellitto, V.M., Sudduth, K.A., Rawlins, B.G., Walter, C., Winowiecki, L.A., Hong, S.Y., Ji, W., 2016b. A global spectral library to characterize the world's soil. Earth-Sci. Rev. 155, 198–230. https://doi.org/10.1016/j.earscirev.2016.01.012.
Viscarra Rossel, R., Bui, E.N., de Caritat, P., Mckenzie, N.J., 2010a. Mapping Iron Oxides and the Color of Australian Soil Using Visible – Near - Infrared Reflectance Spectra. 115. pp. 1–13. https://doi.org/10.1029/2009JF001645.
Viscarra Rossel, R.A., Rizzo, R., Demattê, J.A.M., Behrens, T., 2010b. Spatial modeling of a soil fertility index using visible–near-infrared spectra and terrain attributes. Soil Sci. Soc. Am. J. 74, 1293. https://doi.org/10.2136/sssaj2009.0130.
Wilford, J.R., Searle, R., Thomas, M., Pagendam, D., Grundy, M.J., 2016. A regolith depth map of the Australian continent. Geoderma 266, 1–13. https://doi.org/10.1016/j.geoderma.2015.11.033.
Yamamoto, J.K., 2005. Correcting the smoothing effect of ordinary Kriging estimates. Math. Geol. 37, 69–94. https://doi.org/10.1007/s11004-005-8748-7.
Zeng, R., Zhang, G.-L., Li, D.-C., Rossiter, D.G., Zhao, Y.-G., 2016. How well can VNIR spectroscopy distinguish soil classes? Biosyst. Eng. 152, 117–125. https://doi.org/10.1016/j.biosystemseng.2016.04.019.